Maximal conductances ionic parameters estimation in cardiac electrophysiology multiscale modelling

Yassine Abidi, Julien Bouyssier, Moncef Mahjoub, Nejib Zemzemi

▶ To cite this version:

HAL Id: hal-02154074
https://hal.inria.fr/hal-02154074

Submitted on 13 Jun 2019

Maximal conductances ionic parameters estimation in cardiac electrophysiology multiscale modelling

Yassine Abidi[1][0000−0002−5724−4095], Julien Bouyssier[3][], Moncef Mahjoub[1][0000−0001−7022−493X], and Nejib Zemzemi[2,3][0000−0002−1212−8090]

[1] Tunis El Manar University, ENIT-LAMSIN, Tunis, Tunisia.
[2] INRIA, Bordeaux Sud-Ouest, 200 Avenue de la vielle Tour 33405, Talence Cedex, France.
[3] IHU-LIRYC, Avenue du Haut Lévêque, 33600 Pessac, France.

Abstract. In this work, we present an optimal control formulation for the bidomain model in order to estimate maximal conductances parameters in the physiological ionic model. We consider a general Hodgkin-Huxley formalism to describe the ionic exchanges at the microcopic level. We consider the parameters as control variables to minimize the mismatch between the measured and the computed potentials under the constraint of the bidomain system. The solution of the optimization problem is based on a gradient descent method, where the gradient is obtained by solving an adjoint problem. We show through some numerical examples the capability of this approach to estimate the values of sodium, calcium and potassium ion channels conductances in the Luo Rudy phase I model.

Keywords: parameters estimation, maximal conductance ionic parameters, bidomain model, optimal control with PDE constraints, first order optimality conditions, physiological ionic model, cardiac electrophysiology.

1 Introduction

The bidomain equations are the state-of-the-art model to describe the propagation of the electrical wave in the heart. This model is governed by a system of partial differential equations (PDEs) nonlinearly coupled to a set of non-linear ordinary differential equations (ODEs) describing the dynamics of the cell membrane. These ODEs are usually called the ionic model. The description of these models could be either physiological or phenomenological. In the physiological case, they are in general built using a single cell preparation. Their use in multiscale modeling requires to adjust the parameters. Of particular interest, the ion-channels conductances play an important role in the depolarization rate, the conduction velocity, the repolarization times, ... *etc.* They are key parameters in order to proceed to the personalization of a given model. Given the importance of these parameters, theoretical studies were carried out to establish theoretical stability results for the inverse problem of identification of maximum conductances. Brandao et al. are the first who studied the theoretical analysis and the controllability of the optimization using the FitzHugh-Nagumo model [1]. Later, systematic analysis of the optimal control of monodomain and bidomain model is presented in [2,3,4]. A numerical study for optimal control of the monodomain and the bidomain model allowed to predict optimized shock waveforms in 2D [4] and more recently for the optimal control of bidomain-bath model using Mitchell-Shaeffer model in 3D geometries [5,6]. In those studies the control acts at the boundaries of the bath domain. In an other work [7], authors propose a strategy to optimize a non differentiable cost function obtained from a fit of activation times map. Recently, theoretical studies of the stability of the maximal conductances identification problem in the monodomain [8] and bidomain [9] models have been carried out. Yan and Veneziani proposed a variational procedure for the estimation of cardiac conductivities from measures of the transmembrane and extracellular potentials available at some sites of the tissue [10]. Moreover, the identification from measurements of surface potentials has been tackled in an optimization framework for numerical purposes [11,12]. Recently, drug doses optimization in stem cells preparation has been subject of numerical study following an adjoint procedure [13].

In this study, we propose a variational procedure to the estimation of ionic maximal conductance parameters. The optimal control approach which is based on the minimization of an appropriate cost functional that depends on the maximal conductances and measurments of the transmembrane potentials available at the cardiac tissue. The paper is organized as follows: First, we briefly recall the mathematical equations of the bidomain model describing the electrical wave propagation. In section 3, we present the optimal control formulation approach, a formal derivation of

the adjoint system and the first order optimality condition. The numerical approach to solve the optimality system is explained in Sect 4. Finally, in Sect. 5, we show the numerical results with several test cases and different levels of noise.

2   Mathematical model

Let $\Omega \subset \mathbb{R}^d$ $(d \geqslant 1)$ be a bounded connected open set whose boundary $\Gamma = \partial \Omega$ is regular enough, ($\Omega \subset \mathbb{R}^3$ being the natural domain of the hearth). Let $T > 0$ be a fixed time horizon. We will use the notation $Q = \Omega \times (0, T)$ and $\Sigma = \Gamma \times (0, T)$. We introduce a parabolic-elliptic system called *bidomain model*, coupled to a system of ODEs:

$$
\begin{cases}
A_m\big(C_m \partial_t v + I_{ion}(\bar{\boldsymbol{\varrho}}, v, \mathbf{w}, \mathbf{z})\big) - div(\boldsymbol{\sigma}_i \nabla v) = div(\boldsymbol{\sigma}_i \nabla u_e) + A_m I_{app} & \text{in } Q, \\
-div(\boldsymbol{\sigma}_i \nabla v + (\boldsymbol{\sigma}_i + \boldsymbol{\sigma}_e)\nabla u_e) = 0 & \text{in } Q, \\
\partial_t \mathbf{w} = \boldsymbol{F}(v, \mathbf{w}) & \text{in } Q, \\
\partial_t \mathbf{z} = \boldsymbol{G}(\bar{\boldsymbol{\varrho}}, v, \mathbf{w}, \mathbf{z}) & \text{in } Q, \\
\boldsymbol{\sigma}_i \nabla v . \nu + \boldsymbol{\sigma}_i \nabla u_e . \nu = 0 & \text{on } \Sigma, \\
\boldsymbol{\sigma}_i \nabla v . \nu + (\boldsymbol{\sigma}_i + \boldsymbol{\sigma}_e)\nabla u_e . \nu = 0 & \text{on } \Sigma, \\
v(x, 0) = v_0(x), \;\; \mathbf{w}(x, 0) = \mathbf{w}_0(x), \;\; \mathbf{z}(x, 0) = \mathbf{z}_0(x) & \text{in } \Omega,
\end{cases}
\tag{2.1}
$$

where $v : Q \to \mathbb{R}$ is the transmembrane potential, $u_e : Q \to \mathbb{R}$ is the extracellular electric potential, and $\boldsymbol{\sigma}_i, \boldsymbol{\sigma}_e : \Omega \to \mathbb{R}^{d \times d}$ are respectively the intra- and extracellular conductivity tensors. $\mathbf{w} : Q \to \mathbb{R}^k$ represent the gating variables and $\mathbf{z} : Q \to \mathbb{R}^m$ are the ionic intracellular concentration variables. A_m is the surface to volume ratio of the cardiac cells, and $C_m > 0$ is the membrane capacitance per unit area. $I_{app} : Q \to \mathbb{R}$ is the applied current source and $\bar{\boldsymbol{\varrho}} := \{\bar{\varrho}_i\}_{1 \leqslant i \leqslant N}$ represent a set of maximal conductance parameters. The ionic current I_{ion} and the functions $\boldsymbol{F}$ and $\boldsymbol{G}$ depends of the considered ionic model. In isolated heart conditions, no current flows out of the heart, as expressed by the homogeneous Neumann boundary conditions.

2.1   Membrane models and ionic currents

Following the celebrated work by Hodgkin and Huxley [14], many models of Hodgkin-Huxley (HH) type have later been developed for the cardiac action potential. In these models, the ionic current I_{ion} through channels of the membrane, has the following general structure [15]:

$$
I_{ion}(\bar{\boldsymbol{\varrho}}, v, \mathbf{w}, \mathbf{z}) = \sum_{i=1}^{N} \bar{\varrho}_i y_i(v) \prod_{j=1}^{k} w_j^{p_{j,i}}(v - E_i(\mathbf{z})),
\tag{2.2}
$$

where N is the number of ionic currents, $\bar{\varrho}_i := \bar{\varrho}_i(x)$ is the maximal conductance associated with the ith current, y_i is a gating function depending only on the membrane potentiel v, $p_{j,i}$ are positive integers exponents and E_i is the reversal potential for the ith current, which is the related equilibrium (Nernst) potential and is given by

$$
E_i(\mathbf{z}) = \overline{\gamma}_i \log\left(\frac{z_e}{z_i}\right), \quad \mathbf{z} = (z_1, \ldots, z_m),
\tag{2.3}
$$

where $\overline{\gamma}_i$ is a constant and z_i, $i = 1, \ldots, m$, are the intracellular concentrations. The constant z_e denotes an extracellular concentration. For each action potential model, the dynamic of the gating variables $\mathbf{w}$ and the intracellular concentrations $\mathbf{z}$ are described by a system of ordinary differential equations (ODEs). In this paper, we consider the Luo-Rudy phase I model (LR1) [16] which extends the Beeler-Reuter model [17] to enhance the representation of depolarization and repolarization phases and their interaction. The time course of the action potential (AP) is governed by $N = 6$ ionic currents:

$$
I_{ion} = I_{Na} + I_{si} + I_K + I_{K1} + I_{Kp} + I_b,
\tag{2.4}
$$

which are fast sodium current (I_{Na}), slow inward calcium current (I_{si}), time dependent potassium current (I_K), time independent potassium current (I_{K1}), plateau potassium current (I_{Kp}) and background current (I_b). The time dependent currents I_{Na}, I_{si} and I_K, depend on six activation and inactivation gates m, h, j, d, f, x, and one intracellular concentration variable of Calcium $[Ca^{2+}]_i$, which are governed by ODEs of the form:

$$\frac{dw}{dt} = \alpha_w(v)(1-w) - \beta_w(v)w, \quad \text{for} \ \ w = m, h, j, d, f, x,$$
$$\frac{d}{dt}[Ca^{2+}]_i = -10^{-4}I_{si} + 0.07(10^{-4} - [Ca^{2+}]_i), \tag{2.5}$$

where α_w and β_w are two positive rational functions of exponentials in v. For details on formulation of those functions and the parameters used in our computations, we refer to the original paper of LR1 model [16]. The existence and uniqueness for the LR1 model and more general of the classical HH model of the couple (v, u_e), with u_e has zero average on Ω, i.e $\int_\Omega u_e dx = 0$, can be found in [18].

3   Optimal control problem

In this section, we set the optimal control problem, for which the numerical experiments were carried out. Suppose that v_{meas} is the desired state solution at the cardiac domain, we look for the set/vector of parameters $\bar{\varrho}$ that solves the following minimization problem.

$$(\mathcal{P}) \begin{cases} \min_{\bar{\varrho} \in \mathcal{C}_{ad}} \mathcal{I}(\bar{\varrho}) = \frac{1}{2}\Big(\epsilon_1 \int_Q |v(\bar{\varrho}) - v_{meas}|^2 \, dxt + \epsilon_2 \int_\Omega |\bar{\varrho}|^2 \, dx\Big), \\ \text{subject to the coupled PDE system (2.1), and } \bar{\varrho} \in \mathcal{C}_{ad}, \end{cases} \tag{3.1}$$

where $\mathcal{I}$ is the quantity of interest, ϵ_1 and ϵ_2 are the regularization parameters, v is the state variable and $\int_\Omega |\bar{\varrho}|^2 \, dx$ denotes a Tikhonov-like regularization term used to weigh the impact of the regularization in the minimize procedure. $\mathcal{C}_{ad}$ is the admissible domain for control given by

$$\mathcal{C}_{ad} = \{\bar{\varrho} \in L^\infty(\Omega)^N : \ \bar{\varrho}(x) \in [m, M]^N, \ \forall x \in \Omega\}. \tag{3.2}$$

3.1   Optimal conditions and dual problem

In this paragraph, we formally derive the optimality system associated to (3.1). Let's denote by $\mathcal{J}$ the function

$$\mathcal{J}(\bar{\varrho}, v) = \frac{1}{2}\Big(\epsilon_1 \int_Q |v - v_{meas}|^2 \, dxt + \epsilon_2 \int_\Omega |\bar{\varrho}|^2 \, dx\Big).$$

If $v(\bar{\varrho})$ is solution of (2.1), then we immediately have $\mathcal{J}(\bar{\varrho}, v(\bar{\varrho})) = \mathcal{I}(\bar{\varrho})$. We follow a Lagrangian approach and introduce the following Lagrange functional:

$$\mathcal{L}(v, u_e, \mathbf{w}, \mathbf{z}, \bar{\varrho}, \lambda^*) = \mathcal{J}(\bar{\varrho}, v) - \int_Q pA_m\big(C_m \partial_t v + I_{ion}(\bar{\varrho}, v, \mathbf{w}, \mathbf{z}) - I_{app}\big)dxdt$$
$$- \int_Q p\big(-div(\boldsymbol{\sigma}_i \nabla v) - div(\boldsymbol{\sigma}_i \nabla u_e)\big)dxdt - \int_Q q\big(-div(\boldsymbol{\sigma}_i \nabla v + (\boldsymbol{\sigma}_i + \boldsymbol{\sigma}_e)\nabla u_e)\big)dxdt$$
$$- \int_Q \boldsymbol{r}.\big(\partial_t \mathbf{w} - \boldsymbol{F}(v, \mathbf{w})\big)dxdt - \int_Q \boldsymbol{s}.\big(\partial_t \mathbf{z} - \boldsymbol{G}(\bar{\varrho}, v, \mathbf{w}, \mathbf{z})\big)dxdt, \tag{3.3}$$

where $\lambda^* := (p, q, \boldsymbol{r}, \boldsymbol{s})(x,t)$ denote the Lagrange multipliers. The first order optimality system is given by the Karusch-Kuhn-Tucker (KKT) conditions which result from equating the partial derivatives of $\mathcal{L}$ with respect to the state variables equal to zero. We then obtain the following governing system of the Lagrange multipliers:

$$
\begin{cases}
-A_m(C_m \partial_t p - p \partial_v I_{ion}) - div(\boldsymbol{\sigma}_i \nabla p) - div(\boldsymbol{\sigma}_i \nabla q) - (\partial_v \boldsymbol{F})^T \boldsymbol{r} - (\partial_v \boldsymbol{G})^T \boldsymbol{s} = \epsilon_1(v - v_{meas}) & \text{in } Q, \\
-div(\boldsymbol{\sigma}_i \nabla p + (\boldsymbol{\sigma}_i + \boldsymbol{\sigma}_e) \nabla q) = 0 & \text{in } Q, \\
-\partial_t \boldsymbol{r} + A_m p \partial_{\mathbf{w}} I_{ion} - (\partial_{\mathbf{w}} \boldsymbol{F})^T \boldsymbol{r} - (\partial_{\mathbf{w}} \boldsymbol{G})^T \boldsymbol{s} = 0 & \text{in } Q, \\
-\partial_t \boldsymbol{s} + A_m p \partial_{\mathbf{z}} I_{ion} - (\partial_{\mathbf{z}} \boldsymbol{G})^T \boldsymbol{s} = 0 & \text{in } Q,
\end{cases}
\tag{3.4}
$$

with the terminal conditions
$$
p(x, T) = 0, \quad \boldsymbol{r}(x, T) = \mathbf{0}, \quad \boldsymbol{s}(x, T) = \mathbf{0} \text{ in } \Omega,
\tag{3.5}
$$

and the boundary conditions for the adjoint states

$$
\begin{cases}
-\boldsymbol{\sigma}_i \nabla p . \nu = \boldsymbol{\sigma}_i \nabla q . \nu & \text{on } \Sigma, \\
-\boldsymbol{\sigma}_e \nabla q . \nu = 0 & \text{on } \Sigma.
\end{cases}
\tag{3.6}
$$

In addition, we introduce the compatibility condition for the adjoint variable: $\int_\Omega q(t) dx = 0$, for all $t \in (0, T)$.

Based on the adjoint equations, The gradient of the quantity of interest $\mathcal{I}(\bar{\varrho})$ with respect to $\bar{\varrho}$ reads as follows:

$$
< \frac{\mathcal{DI}}{\mathcal{D}\bar{\varrho}}, \delta\bar{\varrho} > = < \frac{\partial\mathcal{L}}{\partial\bar{\varrho}}, \delta\bar{\varrho} > = \epsilon_2 \int_\Omega \bar{\varrho}.\delta\bar{\varrho} dx - \int_Q A_m p \frac{\partial}{\partial\bar{\varrho}} I_{ion}.\delta\bar{\varrho} dxdt + \int_Q (\frac{\partial\boldsymbol{G}}{\partial\bar{\varrho}})^T \boldsymbol{s}.\delta\bar{\varrho} dxdt,
\tag{3.7}
$$

where $(\frac{\partial\boldsymbol{G}}{\partial\bar{\varrho}})^T$ denotes the transpose of the Jacobian matrix of $\boldsymbol{G} \in \mathbb{R}^m$ in point $\bar{\varrho} \in \mathbb{R}^N$.

4 Numerical approximation

In this section, we give a brief overview of the space and time discretization techniques to solve the primal (2.1) and adjoint (3.4) equations numerically. We use a finite element method (FEM) for the spatial discretization and a semi-implicit Euler scheme for the temporal discretization. We solve the optimal control problem (3.1) using the gradient descent method.

4.1 Space and time discretization:

The semi-discretization of the primal equations in space results in the differential algebraic system as follows:

$$
A_m C_m \boldsymbol{M} \frac{\partial}{\partial t} \boldsymbol{V} = -\boldsymbol{A}_i \boldsymbol{V} - \boldsymbol{A}_i \boldsymbol{U} + A_m \boldsymbol{M}(\mathcal{I}_{app} - \mathcal{I}_{ion}(\bar{\varrho}, \boldsymbol{V}, \boldsymbol{W}^{(j)}, \boldsymbol{Z}^{(j')})),
\tag{4.1}
$$
$$
\boldsymbol{A}_{ie} \boldsymbol{U} = -\boldsymbol{A}_i \boldsymbol{V},
\tag{4.2}
$$
$$
\boldsymbol{M} \frac{\partial}{\partial t} \boldsymbol{W}^{(j)} = \mathcal{F}^{(j)}(\boldsymbol{V}, \boldsymbol{W}^{(j)}),
\tag{4.3}
$$
$$
\boldsymbol{M} \frac{\partial}{\partial t} \boldsymbol{Z}^{(j')} = \mathcal{G}^{(j')}(\bar{\varrho}, \boldsymbol{V}, \boldsymbol{W}^{(j)}, \boldsymbol{Z}^{(j')}),
\tag{4.4}
$$

along with initial conditions for $\boldsymbol{V}, \boldsymbol{W}^{(j)}$ and $\boldsymbol{Z}^{(j')}$, where $\boldsymbol{A}_{ie} = \{< (\boldsymbol{\sigma}_i + \boldsymbol{\sigma}_e)\nabla\omega_i, \nabla\omega_{j''} >\}_{i,j''=1}^M$ and $\boldsymbol{A}_i = \{< \boldsymbol{\sigma}_i \nabla\omega_i, \nabla\omega_{j''} >\}_{i,j''=1}^M$ are the stiffness matrices, $\boldsymbol{M} = \{< \omega_i, \omega_{j''} >\}_{i,j''=1}^M$ is the mass matrix, and $\{\omega_i\}_{i=1}^M$

denote the basis functions, with M is the number of nodal points at the tissue domain. Analogously, the following semi-discrete form of the dual equations is obtained:

$$-A_m C_m \boldsymbol{M}\frac{\partial}{\partial t}\boldsymbol{P} + A_m \boldsymbol{M}(\partial_{\boldsymbol{V}}\boldsymbol{\mathcal{I}_{ion}})^T \boldsymbol{P} = -\boldsymbol{A_i P} - \boldsymbol{A_i Q} + \boldsymbol{M}(\partial_{\boldsymbol{V}}\boldsymbol{\mathcal{F}}^{(j)})^T \boldsymbol{R}^{(j)} + \boldsymbol{M}(\partial_{\boldsymbol{V}}\boldsymbol{\mathcal{G}}^{(j')})^T \boldsymbol{S}^{(j')}$$
$$+ \epsilon_1 \boldsymbol{M}(\boldsymbol{V} - \boldsymbol{V_{meas}}), \tag{4.5}$$

$$\boldsymbol{A_{ie}P} = -\boldsymbol{A_i Q}, \tag{4.6}$$

$$-\frac{\partial}{\partial t}\boldsymbol{R}^{(j)} - (\partial_{\boldsymbol{W}^{(j)}}\boldsymbol{\mathcal{F}}^{(j)})^T \boldsymbol{R}^{(j)} = -A_m(\partial_{\boldsymbol{W}^{(j)}}\boldsymbol{\mathcal{I}_{ion}})^T \boldsymbol{P} + (\partial_{\boldsymbol{Z}^{(j')}}\boldsymbol{\mathcal{G}}^{(j')})^T \boldsymbol{S}^{(j')}, \tag{4.7}$$

$$-\frac{\partial}{\partial t}\boldsymbol{S}^{(j')} - (\partial_{\boldsymbol{Z}^{(j')}}\boldsymbol{\mathcal{G}}^{(j')})^T \boldsymbol{S}^{(j')} = -A_m(\partial_{\boldsymbol{Z}^{(j')}}\boldsymbol{\mathcal{I}_{ion}})^T \boldsymbol{P}, \tag{4.8}$$

with terminal conditions $\boldsymbol{P}(T) = \boldsymbol{R}^{(j)}(T) = \boldsymbol{S}^{(j')}(T) = \boldsymbol{0}, \forall j = 1, \ldots, k, \forall j' = 1, \ldots, m.$

As concerns the time discretization of the primal problem, we start by computing the ODE system in a semi-implicit way: We use a fourth order Runge-Kutta scheme for the computation $\boldsymbol{W}$ and $\boldsymbol{Z}$ while $\boldsymbol{V}$ is kept constant between t and $t + dt$. Then we solve the PDE system $\boldsymbol{V}$ and $\boldsymbol{U}$ sequentially, using a first order semi-implicit scheme where V is taken at time t in the expression of $\mathcal{I}_{ion}$ as in [19]. As concerns the dual equations, although the retrograde problem is fully linear, we use a semi-implicit first order scheme to solve it. The reason is that we separate the ODE system variables $\boldsymbol{R}$ and $\boldsymbol{S}$ from the PDE variables $\boldsymbol{P}$ and $\boldsymbol{Q}$. We also solve the bidomain problem sequentially, we first compute $\boldsymbol{P}$ and then we compute $\boldsymbol{Q}$. This follows the same scheme developed for the primal problem in [19].

4.2 Optimization algorithm

Given an initial guess of maximal conductance parameters $\bar{\varrho}_{guess}$, we solve the optimization problem using the following algorithm based on a gradient descent method.

Algorithm 1 Optimization of the maximal conductance parameters $\bar{\varrho}$

$\bar{\varrho} = \bar{\varrho}_{guess}$,
Solve state problem,
Solve adjoint problem,
while $\mathcal{I}(\bar{\varrho}) > \epsilon_{Func}$ & $\|\frac{\mathcal{DI}}{\mathcal{D}\bar{\varrho}}\| > \epsilon_{Grad}$ & $iter \leqslant MaxIterNumber$ **do**
    $\bar{\varrho} = \bar{\varrho} - \alpha \times \frac{\mathcal{DI}}{\mathcal{D}\bar{\varrho}}$.
    Solve state problem,
    Solve adjoint problem,
    Compute the cost function and its gradient,
end while
$\bar{\varrho}_{opt} = \bar{\varrho}$.

Here, ϵ_{Func} and ϵ_{Grad} are positive constants defining the desired tolerance on the cost function and its gradient respectively. The coefficient α is positive and could be fixed or updated at each iteration and $MaxIterNumber$ stands for the maximal number of iterations in the optimization procedure.

5 Numerical results

In this section, numerical results on the basis of two different test are presented. In all tests, the computational domain $\Omega = [0, 1] \times [0, 1] \subset \mathbb{R}^2$ of size 0.1×0.1 cm^2 is fixed and a triangular discretization is used with the mesh parameter $h \approx 25 \mu m$ which consists of 11508 elements and 5835 nodes. The stimulation current is imposed in the right bottom
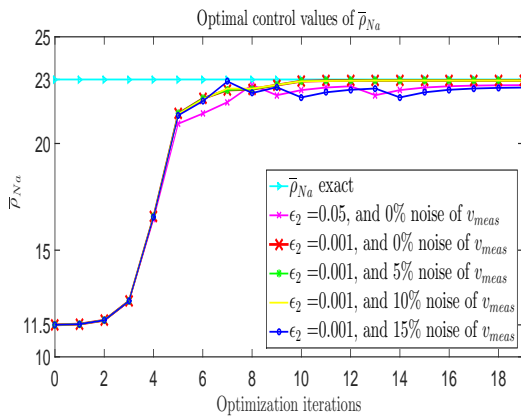
corner of the geometry its magnitude is $I_{app}(t) = 80\mu A/cm^2$ and its duration is 1ms. During the simulations, we fix the time step length $\Delta t = 0.1ms$. The termination of the optimization algorithm is based on the following condition:

$$\epsilon_{Func} = 10^{-8} \text{ and } \epsilon_{Grad} = 10^{-6}. \tag{5.1}$$

Moreover, if these conditions are not satisfied, the algorithm terminates within a prescribed number of iterations. Here the maximum number of iteration parameter is $MaxIterNumber = 20$. For all the following tests, the desired transmembrane potential v_{meas} are simulated with the physiological Luo Rudy phase I model with its original control parameters. There are six ionic currents in the Luo Rudy phase I model I_{Na}, I_{si}, I_{K1}, I_K, I_{Kp} and I_b. Each of the currents has its corresponding maximal ion-channel conductance $\bar{\varrho}_{Na}$, $\bar{\varrho}_{si}$, $\bar{\varrho}_{K1}$, $\bar{\varrho}_K$, $\bar{\varrho}_{Kp}$ and $\bar{\varrho}_b$. In what follows, we will consider to optimize three of them $\bar{\varrho}_{Na}$, $\bar{\varrho}_{si}$, $\bar{\varrho}_{K1}$ representing three different ion channels: sodium, calcium and potassium, respectively.

5.1 Test 1: Optimize the maximal conductance parameter of the fast inward sodium current $\bar{\varrho}_{Na}$:

In this test, we present a numerical results of the estimation of the parameter $\bar{\varrho}_{Na}$. Since this parameter is mainly important in the depolarization phase, we consider the cost function in the time window $[0ms, 20ms]$ of the simulation. The exact value $\bar{\varrho}_{Na}$ is equal to 23. We generate the measurement v_{meas} by solving the forward problem using the exact value of $\bar{\varrho}_{Na}$ and we start our optimization procedure using a guess value $\bar{\varrho}_{Na,guess} = \frac{1}{2}\bar{\varrho}_{Na} = 11.5$. Since the cost function depends on the parameters ϵ_1 and ϵ_2 used to make a balance between the function of interest $(\int_Q |v(\bar{\varrho}_{Na}) - v_{meas}|^2 dxt)$ and the regularization term $(\int_\Omega |\bar{\varrho}_{Na}|^2 dx)$, we first run the optimization procedure with $\epsilon_1 = 1$ and we vary ϵ_2 from 0.05 to 0.001. As shown in Fig 1, for both cases the optimization algorithm converges to the desired control value. But the accuracy is better with $\epsilon_2 = 0.001$ than $\epsilon_2 = 0.05$ as shown in Table1. From now on we fix $\epsilon_1 = 1$ and $\epsilon_2 = 0.001$.

Fig. 1: The optimal control solution for the optimization of $\bar{\varrho}_{Na}$ for different values of ϵ_2 and different levels of noise.

ϵ_2	Noise on v_{meas} (%)	$\frac{\|\bar{\varrho}_{Na,exact} - \bar{\varrho}_{Na}\|}{\|\bar{\varrho}_{Na,exact}\|} \times 10^2$
0.05	0 %	1.117 %
0.001	0 %	0.195 %
0.001	5 %	0.196 %
0.001	10 %	0.22 %
0.001	15 %	1.58 %

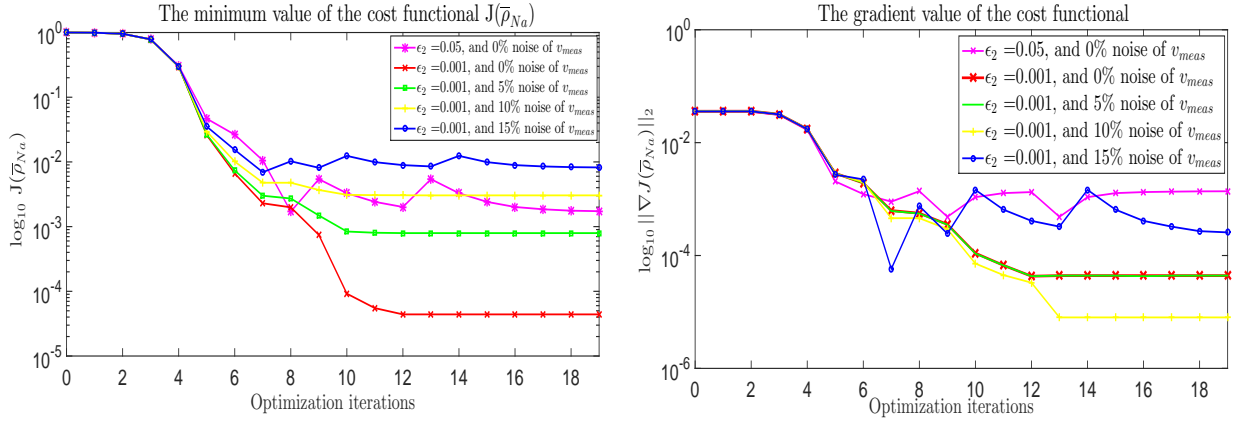Table 1: Relative error for all cases.

Fig. 2: Left: Log scale plot of the cost function $\mathcal{I}(\bar{\varrho}_{Na})$. Right: Log scale plot of the norm of its gradient during the optimization procedure.

In order to test the robustness of the algorithm, we add different levels of gaussian noise to the measured data v_{meas}, and we solve the optimization problem following Algorithm 1 for each value of noise. As shown in Fig 1, the algorithm converges for all levels of noise. Table1 shows that the accuracy is altered with the noise. But for 15% of noise, the relative error on the estimated value of $\bar{\varrho}_{Na}$ is under 2%. Figure 2 shows the evolution of the cost function $\mathcal{I}(\bar{\varrho}_{Na})$ and the norm of its gradient with respect to the optimization iterations for different regularization parameter values ϵ_2 and noise levels on the measured potential.

5.2   <u>Test 2: Optimize the maximal conductance parameter of the slow inward-calcium related current $\bar{\varrho}_{si}$:</u>

In this test, we present a numerical results for the optimization of the parameter $\bar{\varrho}_{si}$. Since this parameter acts on the plateau phase, we performed the optimization on a time window [0ms, 400ms]. We consider the initial guess value $\bar{\varrho}_{si,guess} = \dfrac{3}{2}\bar{\varrho}_{si,exact} = 0.135$. Fig 3 (left) shows the evolution of the parameter $\bar{\varrho}_{si}$ during the optimization procedure. The table in Fig 3 (right) shows the relative error of the obtained solution with respect to the 0%, 5% and 10% noise levels. We can see that it converge from the fourth iteration and the accuracy of the obtained optimal solution of $\bar{\varrho}_{si}$ seems to be less sensitive to noise compared to optimal solution of $\bar{\varrho}_{Na}$.

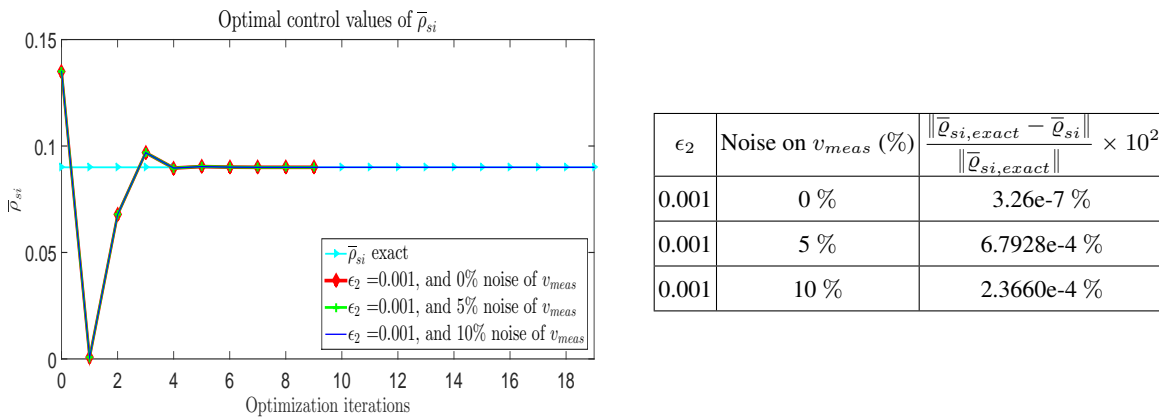| ϵ_2	Noise on v_{meas} (%)	$\dfrac{\|\bar{\varrho}_{si,exact} - \bar{\varrho}_{si}\|}{\|\bar{\varrho}_{si,exact}\|} \times 10^2$
0.001	0 %	3.26e-7 %
0.001	5 %	6.7928e-4 %
0.001	10 %	2.3660e-4 %

Fig. 3: Left: The evolution of the optimal control solution $\bar{\varrho}_{si}$ during the optimization iteration. Right: Relative errors of the optimal control solution for different noise levels.

5.3   Test 3: Optimize the maximal conductance parameter of the time-independent potassium current $\bar{\varrho}_{K1}$:

In this test, we present a numerical results for the optimization of the parameter $\bar{\varrho}_{K1}$. Since this parameter acts on the repolarization phase, we performed the optimization on a time window [0ms, 400ms]. The initial guess considered is $\bar{\varrho}_{K1,guess} = \frac{3}{2}\bar{\varrho}_{K1,exact} = 0.90705$. Fig 4 (left) shows the evolution of the parameter $\bar{\varrho}_{K1}$ during the optimization procedure. The table in Fig 4 (right) shows the relative error of the obtained solution with respect to the noise level. The results in the table show that the optimal solution of $\bar{\varrho}_{K1}$ is more sensitive to the noise than $\bar{\varrho}_{si}$ and less sensitive to noise than $\bar{\varrho}_{Na}$.

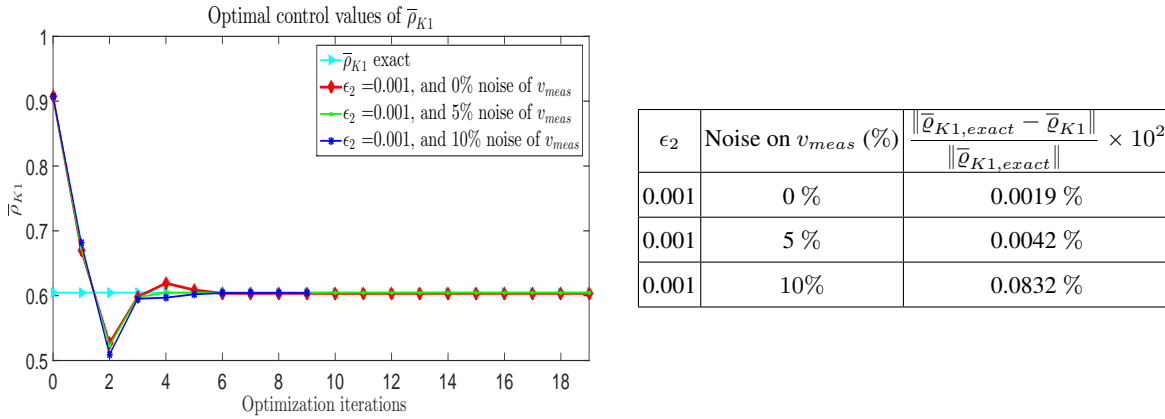| ϵ_2	Noise on v_{meas} (%)	$\dfrac{\|\bar{\varrho}_{K1,exact} - \bar{\varrho}_{K1}\|}{\|\bar{\varrho}_{K1,exact}\|} \times 10^2$
0.001	0 %	0.0019 %
0.001	5 %	0.0042 %
0.001	10%	0.0832 %

Fig. 4: Left: The evolution of the optimal control solution $\bar{\varrho}_{K1}$ during the optimization iterations. Right: Relative errors of the optimal control solution for different noise levels.

6   Discussion and conclusions

In this paper, we have presented an approach for the estimation of maximal conductance parameters of the Luo Rudy phase I model. We formulated the problem as an optimization procedure in an optimal control problem where the cost function represents the misfit between the measured signals and the model. Our numerical results shows the capability of this method to estimate the maximal conductance parameter $\bar{\varrho}_{Na}$ (respectively, $\bar{\varrho}_{si}$, $\bar{\varrho}_{K_1}$) of the fast sodium current (respectively, slow inward and potassium currents). This study shows also that the optimization procedure is robust with respect of noise. Although, results show also that the optimization of $\bar{\varrho}_{Na}$ is more sensitive to noise than it is for $\bar{\varrho}_{si}$ and $\bar{\varrho}_{K1}$. The challenge is to explore the capability of this method to estimate these physiological parameters when dealing with real life measurement. Finally, we have to say that this study is preliminary and that we didn't explore all of the potential of the optimal control approach. The method here presented allows multiple parameter estimation. It also allows the estimation of space dependent parameters. This would be subject of our future research.

Acknowledgements

References

1. A. J. Brandao, E. Fernandez-Cara, P. Magalhaes, and M. A. Rojas-Medar. Theoretical analysis and control results for the fitzhugh-nagumo equation. *Electronic Journal of Differential Equations (EJDE)[electronic only]*, 2008:Paper–No 164, 2008.

2. E. Casas, C. Ryll, and F. Tröltzsch. Sparse optimal control of the schlögl and fitzhugh-nagumo systems. *Computational Methods in Applied Mathematics*, 13(4):415–442, 2013.

3. K. Kunisch and M. Wagner. Optimal control of the bidomain system (iii): Existence of minimizers and first-order optimality conditions. *ESAIM: Mathematical Modelling and Numerical Analysis*, 47(4):1077–1106, 2013.

4. N. Chamakuri, K. Kunisch, and G. Plank. Numerical solution for optimal control of the reaction-diffusion equations in cardiac electrophysiology. *Computational Optimization and Applications*, 49(1):149–178, 2011.

5. N. Chamakuri and K. Kunisch. Primal-dual active set strategy for large scale optimization of cardiac defibrillation. *Applied Mathematics and Computation*, 292:178–193, 2017.

6. M. Bendahmane, N. Chamakuri, E. Comte, and B. Ainseba. A 3d boundary optimal control for the bidomain-bath system modeling the thoracic shock therapy for cardiac defibrillation. *Journal of Mathematical Analysis and Applications*, 437(2):972 – 998, 2016.

7. D. Ngoma, P. Vianney, Y. Bourgault, and H. Nkounkou. Parameter identification for a non-differentiable ionic model used in cardiac electrophysiology. *Applied Mathematical Sciences*, 9(150):7483–7507, 2015.

8. Y. Abidi, M. Bellassoued, M. Mahjoub, and N. Zemzemi. On the identification of multiple space dependent ionic parameters in cardiac electrophysiology modelling. *Inverse Problems*, 34(3):035005, 2018.

9. Y. Abidi, M. Bellassoued, M. Mahjoub, and N. Zemzemi. Ionic parameters identification of an inverse problem of strongly coupled pdes system in cardiac electrophysiology using carleman estimates. *Math. Model. Nat. Phenom.*, 14(2):202, 2019.

10. H. Yang and A. Veneziani. Estimation of cardiac conductivities in ventricular tissue by a variational approach. *Inverse Problems*, 31(11):115001, 2015.

11. C. E. Chávez, N. Zemzemi, Y. Coudière, F. Alonso-Atienza, and D. Alvarez. Inverse problem of electrocardiography: Estimating the location of cardiac ischemia in a 3d realistic geometry. In *International Conference on Functional Imaging and Modeling of the Heart*, pages 393–401. Springer, 2015.

12. B. F. Nielsen, M. Lysaker, and A. Tveito. On the use of the resting potential and level set methods for identifying ischemic heart disease: An inverse problem. *Journal of computational physics*, 220(2):772–790, 2007.

13. J. Bouyssier and N. Zemzemi. Parameters estimation approach for the mea/hipsc-cm asaays. In *2017 Computing in Cardiology (CinC)*, pages 1–4. IEEE, 2017.

14. A. L. Hodgkin and A. F. Huxley. A quantitative description of membrane current and its application to conduction and excitation in nerve. *The Journal of Physiology*, 117(4):500–544, 1952.

15. P. C. Franzone L. F. Pavarino and S. Scacchi. *Mathematical Cardiac Electrophysiology*. Springer International Publishing, 2014.

16. C. H. Luo and Y. Rudy. A model of the ventricular cardiac action potential: Depolarization, repolarization, and their interaction. *Circulation Research*, 68(6):1501–1526, 1991.

17. G. W. Beeler and H. Reuter. Reconstruction of the action potential of ventricular myocardial fibres. *The Journal of Physiology*, 268(1):177–210, 1977.

18. M. Veneroni. Reaction-diffusion systems for the macroscopic bidomain model of the cardiac electric field. *Nonlinear Analysis: Real World Applications*, 10:849–868, 2009.

19. MA. Fernández and N. Zemzemi. Decoupled time-marching schemes in computational cardiac electrophysiology and ecg numerical simulation. *Mathematical biosciences*, 226(1):58–75, 2010.